Construction and Building Materials 411 (2024) 134757

Contents lists available at ScienceDirect

Construction and Building Materials

journal homepage: www.elsevier.com/locate/conbuildmat

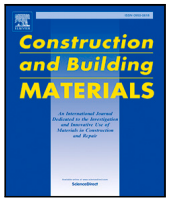

A computationally efficient procedure for calibrating model parameters of multiple specimens

Loris Vincenzi [a], Federico Ponsi [b], Elisa Bassoli [a,*], Nicola Buratti [b]

[a] University of Modena and Reggio Emilia, Department of Engineering "Enzo Ferrari" (DIEF), Modena, Italy
[b] University of Bologna, Department of Civil, Chemical, Environmental and Materials Engineering (DICAM), Bologna, Italy

ARTICLE INFO

Keywords:
Model parameter calibration
Multiple specimens
Surrogate assisted algorithm
Fiber Reinforced Concrete

ABSTRACT

Model calibration can be a very intensive and time-consuming task, especially when dealing with non-linear and large finite element models. The computational effort further increases when multiple specimens have to be calibrated. This is typical of laboratory experiments where several specimens made with the same and/or different constituent materials are tested. This paper proposes a calibration procedure aimed at reducing the computational effort of multiple specimen model calibration. The calibration procedure combines the robustness of a surrogate-assisted evolutionary algorithm with the exploitation of a database collecting the results of the previously calibrated specimens. In this research, the proposed procedure is applied to the calibration of the parameters of a cohesive crack model for fiber-reinforced concrete specimens. The benefit of the proposed procedure is shown by comparing the results with those obtained from the same calibration method but without accounting for the previous results in the calibration of a new specimen.

1. Introduction

Inverse analyses are widely employed for the calibration of material mechanical models [1]. The direct definition of their parameters from experimental test is often unfeasible, in particular for complex models. Therefore, in many applications parameters are estimated by minimizing the difference between the measures obtained from an experimental test and the corresponding responses obtained from a simulation model, e.g. a finite element (FE) model. This approach is very suited for the calibration of non-linear mechanical models describing the behavior of cementitious materials (see, for instance, [2,3]). Due to the difficulties in performing uniaxial tension tests [4], model parameters are usually estimated through inverse analyses based on the results of a three point bending test (TPBT) performed on a notched beam or of a wedge splitting test (WST) [5]. The specimen response to a WST is commonly simulated through FE models [6–8], while for a TPBT both closed form solutions [9–13] and numerical simulations [8,14] have been developed. Among these models, the fictitious crack model proposed by Hillerborg [15] is probably one of the most commonly adopted. However, other similar models can be found in literature, such as the cracked band model by Bazant and Oh [16].

Once the mechanical model describing the material behavior is defined, a proper strategy is required to evaluate the model parameter values that ensure the minimum discrepancy between experimental and numerical outcomes. A global approach can be adopted, involving the simultaneous optimization of all parameters defining the mechanical model. In this case, the simplest way to proceed is to use a trial-and-error procedure or a manual parametric study [17–19]. However, these approaches are not efficient and their results may be far from the desired accuracy. Hence, specific calibration procedures based on optimization algorithms able to find the best solution by minimizing the differences between numerical and experimental results need to be employed. To this purpose, both gradient-based [7,12] and non gradient-based algorithms [20,21] have been adopted in literature. de Oliveira and Gettu [12] proposed a weighted objective function to be minimized with a gradient-based algorithm combined with line search techniques. The convergence rate is improved by using the Newton–Raphson algorithm or the steepest descent method depending on whether the Hessian matrix is positive definite or not. On the other hand, Buratti et al. [21] employed the genetic optimization algorithm implemented in Matlab to solve the inverse problem. The corresponding numerical curve was in good agreement with the experimental results presented in the same article. A possible alternative to these approaches is the sequential optimization, where subsets of parameters are calibrated in different phases and on the basis of different subsets of data [8,13,17]. Sequential optimization can be successfully applied when the number of constitutive parameters to compute is high and

* Corresponding author.
E-mail address: elisa.bassoli@unimore.it (E. Bassoli).

https://doi.org/10.1016/j.conbuildmat.2023.134757
Received 15 May 2023; Received in revised form 22 December 2023; Accepted 23 December 2023
Available online 27 December 2023

the optimization can result in an ill-conditioned problem. However, the sequential optimization of parameter subsets may lead to a local minimum rather than to the global one. Jepsen et al. [22] proposed an adaptive method aimed at constructing a multi-linear softening curve. First, a bi-linear curve is used for the fitting, then edge points are sequentially added to the curve one by one in accordance with a refinement criterion. An interesting application of the Kalman filter in this field was proposed by Bolzon et al. [6], thus enabling the uncertainty quantification associated with the estimated parameters.

Unfortunately, model calibration is a very time consuming task, especially when dealing with non-linear and/or large FE models (e.g. [23, 24]). Although a single analysis with such models may not be excessively time consuming, the model calibration procedure involving an iterative process may become very computationally expensive. Moreover, TPBTs or WSTs are usually performed on a series of specimens that can be arranged in groups according to their properties. Each group can be composed of several specimens with the same properties. In this situation, several mechanical models need to be calibrated to investigate both the effect of different constituent materials and the variability of model parameters for specimens of the same group. In this case, multiple optimization problems must be solved and the computational effort may become excessive. Although the calibration of multiple specimens is very recurring in the research activity, the literature lacks studies aimed at reducing its computational cost.

In this demanding context, this paper proposes a procedure to reduce the computational effort of model calibration when dealing with multiple specimens, each one with the same geometry but with different constituent materials. In particular, the procedure exploits the results obtained from the calibration of each single specimen to guide the calibration of new specimens. Each specimen calibration is performed through a surrogate-assisted evolutionary algorithm combined with an improved sampling strategy [25]. The basic idea for an efficient model calibration of multiple specimens is the following: all the parameter values investigated in each specimen calibration are stored in a database so that the calibration of each new specimen can start from the database values rather than from randomly generated samples. This allows guiding the research of the optimal model parameters on the basis of the calibration results obtained for previous specimens, thus reducing the number of model evaluations required. The proposed procedure is able to reduce the model evaluations required while the robustness in the global minimum search is guaranteed by the use of an efficient evolutionary algorithm.

The proposed procedure is applied in this study to the calibration of the constitutive models of multiple fiber-reinforced concrete (FRC) specimens, characterized by the same geometry and varying concrete strength and fiber dosage. The distinctive contribution of this work is the development of an efficient calibration procedure and it is not limited to the specific presented case study. This procedure can be extended to any case where a numerical model has to be calibrated on the basis of experiments performed on multiple specimens with the same geometrical characteristics. The number of parameters to be calibrated in a single optimization problem is not theoretically limited, provided that the problem is well-posed, namely its solution exists, is unique, and continuously depends on errors present in the problem formulation [26]. The only drawback related to an increasing number of calibration parameters is the resulting increased computational time. The proposed approach can be employed to identify model parameters for design applications [21] or to calibrate advanced non-linear models for research purposes [24].

The paper is organized as follows. First, the experiments on the FRC specimens, their mechanical modeling and the objective function defined for model calibration purposes are introduced in Section 2. The procedure proposed for the calibration of multiple specimens is described in Section 3, while the calibration results are presented and discussed in Section 4. Finally, conclusions are drawn in Section 5.

2. Calibration of stress–crack opening relationship for FRC specimens

This section describes the experimental tests performed on the FRC specimens, the model adopted to characterize their mechanical behavior and the objective function defined for the model parameter calibration. The mechanical model is a non-linear stress–crack opening relationship whose parameters are calibrated through the optimization procedure described in Section 3. In the present paper, the proposed calibration algorithm is applied to FRC elements in bending, because, for this material, specimens that have the same geometry and fiber dosage, and are made from the same concrete batch, tend to have significantly different mechanical responses due to the random distribution of fibers. Therefore, numerical model calibration is performed on each specimen in order to investigate the variability of the numerical model parameters.

2.1. Experimental tests

The experimental campaign is carried out on $150 \times 150 \times 550$ mm^3 prismatic specimens cast with different concretes and fiber dosages. Crimped polypropylene fibers with a length of 39 mm and an equivalent diameter of 0.92 mm are used. Each specimen is tested in a three-point bending scheme and is notched at mid-span in order to control the crack triggering, according to EN 14651. A clip-on displacement transducer is installed at the bottom of the specimen, across the notch, in order to measure the Crack Mouth Opening Displacement (CMOD). Test are carried out in CMOD control with a servo-hydraulic testing machine, with an opening rate of 0.05 mm/min for CMOD $<$ 0.1 mm and 0.1 mm/min for larger CMOD values. A picture of the experimental setup is shown in Fig. 1(a), while Fig. 1(b) presents an example of a force–CMOD curve obtained from one of the tests. A total of 63 specimens are tested, they are classified in the following based on the compressive strength of the concrete (with strength varying from 34 MPa to 55 MPa), and on the fiber dosage (4, 6 and 8 kg/m^3). For each dosage of fibers three different batches of 7 specimens are produced, the compressive strength is assumed constant for each batch and is measured by means of tests on two cubes. In particular, the following 9 specimen groups are identified: F4-C54, F4-C47, F4-C41, F6-C55, F6-C43, F6-C34, F8-C41, F8-C39, F8-C37, where Fx denotes the fiber dosages and Cxx the concrete compressive strength. The 7 specimens of each batch are referred to as T1–T7. According to this classification, the force–CMOD curve shown in Fig. 1(b) refers to the first specimen (T1) of the group characterized by 54 MPa of concrete compressive strength and a fiber dosage of 4 kg/m^3. The specimens are made with the main objective of obtaining a sufficiently large number of different force–CMOD curves in order to test the advantages of the algorithm proposed in the following. No particular target in terms of strength was set.

2.2. Numerical model

The three point bending tests are modeled by means of a 2D FE model using the software Abaqus. Exploiting the symmetry of the problem, only half of the specimen is modeled, using four-node plane-stress elements (type CPS4R in Abaqus) with an elastic isotropic material. The crack propagation is simulated using a simple cohesive crack model, by means of nonlinear springs (see Fig. 2(a)) with a very high elastic stiffness in tension and compression. The high initial stiffness of the springs is necessary so as not to add further elastic deformability to the system, whose overall elastic deformability is simulated through the elastic 2D elements. The adopted mesh is depicted in Fig. 2(b). In the crack zone the elements are square with an edge size of 2 mm. The analysis is conducted under displacement control by increasing with a small step size the vertical displacement of the beam midspan and by recording the corresponding values of force and CMOD. During the

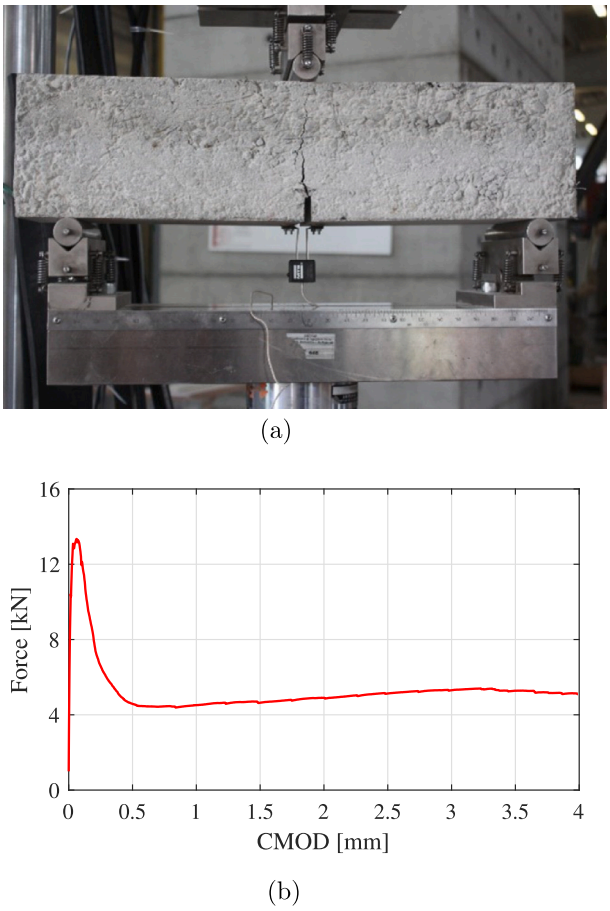

Fig. 1. (a) The experimental setup and (b) the force–CMOD experimental curve of the specimen F4-C54-T1.

analysis, when the tensile stress in one of the nonlinear springs equates the tensile strength of concrete f_{ct}, the crack opens/propagates, and the stress in the spring is described based on the stress (σ)-crack opening (w) relationship

$$\sigma(w) = g_1(w) + g_2(w) = a_1\left(e^{-a_2 w}\right) + a_3\left(e^{-a_4 w} - e^{-a_5 w}\right) \quad (1)$$

where a_1 to a_5 are unknown parameters. The exponential curve of Eq. (1) is adapted from [27]. The overall trend of Eq. (1) and the partial contribution of $g_1(w)$ and $g_2(w)$ are shown in Fig. 3 . Note that $g_1(w)$ describes mainly the crack propagation in concrete, while $g_2(w)$ (and the parameters a_3-a_5) characterize the effect of the fibers. Since $\sigma(w) = a_1$ when $w = 0$, the parameter a_1 represents the tensile strength of concrete f_{ct}. Clearly, in the adopted model the elongation of a certain nonlinear spring represents one half of the crack opening at the location of the spring. Moreover, as mentioned before, the elastic behavior of concrete in tension before cracking is simulated by the quadrilateral plane stress elements.

It should be noticed that many stress–crack opening relationships have been proposed in the literature [28]; the one adopted here (Eq. (1)) was chosen in the first place because it depends on 5 parameters and therefore it is associated to a certain complexity of the optimization problem. In the second place, it allows to describe the shape of the experimental curves with a good accuracy, with particular reference to the second peak observed in the force–crack opening relationship (see Fig. 1(b)). In the present work the numerical model is functional to application of the calibration algorithm. Clearly more advanced models are available in the literature [29,30], but their adoption would not change the conclusions of the present work on the efficiency of the proposed calibration algorithm.

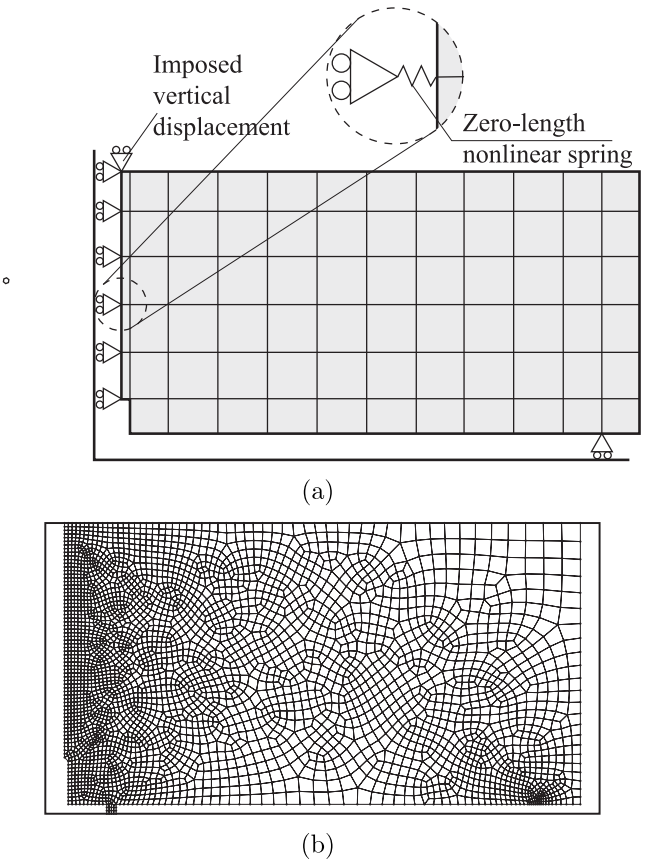

Fig. 2. (a) Schematic view of the numerical model and (b) FE model mesh.

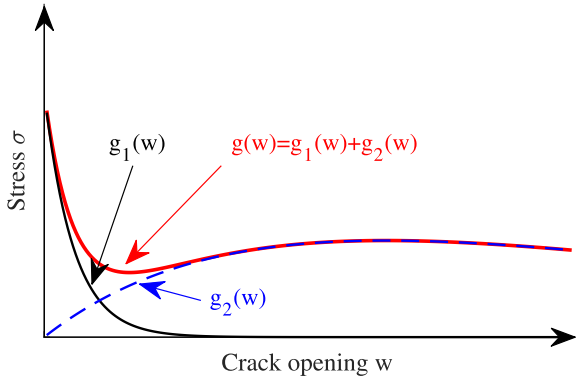

Fig. 3. Stress–crack opening relationship of Eq. (1). Continuous black line: $g_1(w)$, dashed blue line: $g_2(w)$, bold red line: $g(w)$. (For interpretation of the references to color in this figure legend, the reader is referred to the web version of this article.)

2.3. Definition of the objective function

The aim of the calibration procedure is to find the optimal vector $\mathbf{a} = \{a_1, \ldots, a_5\}$ composed of the 5 parameters of the constitutive law (Eq. (1)) that best approximates an experimental test. It should be noticed that the elastic modulus of the concrete is not included in the optimization process because it has a limited effect on the force–CMOD curves after the first peak. A value of 37,200 MPa is used. The choice of the objective function H for the optimization problem is crucial for the success of the calibration procedure [31,32]. In this paper, the objective function is defined as the weighted sum of three squared residuals between experimental results, indicated with the (ex)

superscript, and numerical results, indicated with the (n) superscript, in terms of force–CMOD curves:

$$H(\mathbf{a}) = k_1 e_F^2 + k_2 e_A^2 + k_3 e_{\text{CMOD}}^2 \tag{2}$$

where e_F^2 is the squared residual in terms of maximum force $F_{\max}$, defined as

$$e_F^2 = \left(\frac{F_{\max}^{(\text{ex})} - F_{\max}^{(\text{n})}(\mathbf{a})}{F_{\max}^{(\text{ex})}} \right)^2 \tag{3}$$

e_A^2 measures the residual in terms of area A under the force–CMOD curves in the interval 0.03 mm ≤ CMOD ≤ 3.5 mm and is defined as

$$e_A^2 = \left(\frac{A^{(\text{ex})} - A^{(\text{n})}(\mathbf{a})}{A^{(\text{ex})}} \right)^2 \tag{4}$$

and e_{CMOD}^2 is the average residual at N different reference CMOD values

$$e_{\text{CMOD}}^2 = \frac{1}{N} \sum_{h=1}^{N} \left(\frac{F^{(\text{ex})}(\text{CMOD}_h) - F^{(\text{n})}(\text{CMOD}_h, \mathbf{a})}{F^{(\text{ex})}(\text{CMOD}_h)} \right)^2 \tag{5}$$

In this study, $N = 8$ and the reference CMOD values are CMOD_1 = 0.03 mm, CMOD_2 = 0.05 mm, CMOD_3 = 0.1 mm, CMOD_4 = 0.2 mm, CMOD_5 = 0.5 mm, CMOD_6 = 1.5 mm, CMOD_7 = 2.5 mm, CMOD_8 = 3.5 mm. The wights in Eq. (2) are set as follows: $k_1 = k_2 = k_3 = 1$.

Given an experimental force–CMOD curve, the goal of the calibration is to find the set of parameters $\mathbf{a}$ that minimizes the objective function Eq. (2), thus minimizing the discrepancy between the experimental and the numerical findings. The algorithm does not involve the calibration of unique parameter values for a set of nominally equal specimens. Indeed, in this case it would not be possible to estimate the model parameter variability due to the random distribution of fibers inside the concrete matrix. The optimization is thus carried out independently for each specimen.

3. Calibration of multiple specimens

The proposed calibration procedure combines the robustness of a surrogate-assisted evolutionary algorithm and the efficiency related to the exploitation of a database of results. This latter is built during the calibration procedure and allows reducing the number of model evaluations required to calibrate the numerical model based on the results obtained from multiple specimens. The surrogate-assisted evolutionary algorithm is presented in Section 3.1 with reference to the calibration of a single specimen, while the efficient procedure for the calibration of multiple specimens is described in Section 3.2.

3.1. The surrogate-assisted evolutionary algorithm

The surrogate-assisted evolutionary algorithm employed in this paper was originally proposed by one of the authors [25,33] and is based on the use of the differential evolution (DE) algorithm [34] combined with a second order polynomial surrogate and two scoring criteria to improve the performance of the original DE algorithm. The DE algorithm is a parallel direct search method widely employed in the field of numerical optimization. The basic procedure of the DE algorithm is reported in detail in [34], while a description of the surrogate-assisted strategy is presented in the following.

The calibration parameters a_i are collected in the D-dimensional vector $\mathbf{a} = \{a_1, \dots, a_i, \dots, a_D\}$ ($D = 5$ in the present work) and the aim of the calibration procedure is to find the optimal value of $\mathbf{a}$ that ensures the minimum value of the objective function of Eq. (2). At each iteration G of the calibration procedure, a set of N_P parameter vectors is defined according to the criteria described in the following. Hence, at each iteration G the population is composed of N_P parameter vectors $\mathbf{a}_{j,G}$ (with $j = 1, \dots, N_P$), each one representing a point in the D-dimensional search domain. The N_P parameter vectors of the Gth iteration are referred to as generation G.

When dealing with the calibration of the first specimen, the first generation of parameter vectors ($G = 1$) is randomly chosen in the research domain. The objective function value $H(\mathbf{a}_{j,1})$ corresponding to the jth parameter vector of the initial population is evaluated using Eq. (2). Notice that the numerical quantities $F_{\max}^{(n)}$, $A^{(n)}$ and $F^{(n)}(\text{CMOD}_h)$ in Eq. (2) are obtained by running the FE model described in Section 2.2 with the model parameters $\mathbf{a}_{j,1}$. Once the objective function values $H(\mathbf{a}_{j,1})$ for each of the N_P first generation parameter vectors are computed, the surrogate-assisted algorithm generates the N_P parameter vectors of the new generation trying to establish a balance between local and global search. This means to enhance both the accuracy of the solution in the neighboring of the optimum predicted at the previous iteration (local exploitation) and the global optimum search (global exploration).

The local exploitation is performed by means of a second order polynomial surrogate function, used to approximate the objective function H with the objective of improving the convergence speed to the global minimum. In the proposed algorithm, a second order polynomial function is selected because it can locally fit the objective function H and its minimizer can be calculated analytically (i.e. without any iterative process). The definition of the surrogate function is detailed in Section 3.1.1.

The global exploration is performed by combining the parameter vectors $\mathbf{a}_{j,G}$ belonging to the same G-generation to explore the search space and to avoid reaching local minima. According to the classic DE algorithm, a linear combination of the vectors $\mathbf{a}_{j,G}$ is used.

Each new parameter vector defined by the two above described strategies is assigned a score in order to select only the ones that are either likely to provide new information on the research domain or that are characterized by lower objective function values. To this aim, the N_H vectors characterized by the lowest score are selected and their corresponding objective function values are calculated. The influence of N_H on the speed rate of the algorithm is evaluated in [25], where an optimal value of about 4 or 5 is proposed. Details about the score assignment are presented in Section 3.1.2.

A new parameter vector is part of the next generation population only if its corresponding objective function value is lower than one of the vectors of the current generation. The algorithm proceeds for successive iterations until prescribed convergence criteria are reached.

At each iteration, all vectors $\mathbf{a}_{j,G}$ constituting the generation G, the corresponding objective function values $H(\mathbf{a}_{j,G})$ and the numerical results (namely the force–CMOD curve obtained from the FE model with $\mathbf{a}_{j,G}$ in this research) are stored in a database. This database is used in the calibration of a single specimen for scoring purposes (see Section 3.1.2) as well as to calibrate multiple specimens (Section 3.2). A flowchart of the surrogate-assisted evolutionary algorithm is presented in Fig. 4.

3.1.1. Surrogate definition

The N_P parameter vectors of the generation G are starting points for the definition of the next generation of vectors. This is achieved according to two strategies. The first is the classic strategy of the DE algorithm [34], based on the mutation (linear combination of vectors) and crossover (combination of the mutant vector and original vector components) operations. The second strategy adopted in this research is based on surrogate functions and detailed in the following. At each iteration G, N_P subsets of vectors, each one composed of N_S vectors (with $N_S < N_P$), are randomly generated. The number of subsets N_S is defined based on the dimension of the search space, the value adopted in the present paper is discussed in Section 4. For each vector, the corresponding value of the objective function $H(\mathbf{a}_{j,G})$ is known (i.e. the FE model is run, numerical results are known and $H(\mathbf{a}_{j,G})$ is calculated). For each subset of N_S vectors, a second-order polynomial surrogate function $\overline{H}$ is calibrated to obtain an estimate of the objective function H:

$$\overline{H}(\mathbf{a}_{j,G}) = \frac{1}{2} \mathbf{a}_{j,G}^T \mathbf{Q}\, \mathbf{a}_{j,G} + \mathbf{l}\, \mathbf{a}_{j,G} + c \tag{6}$$

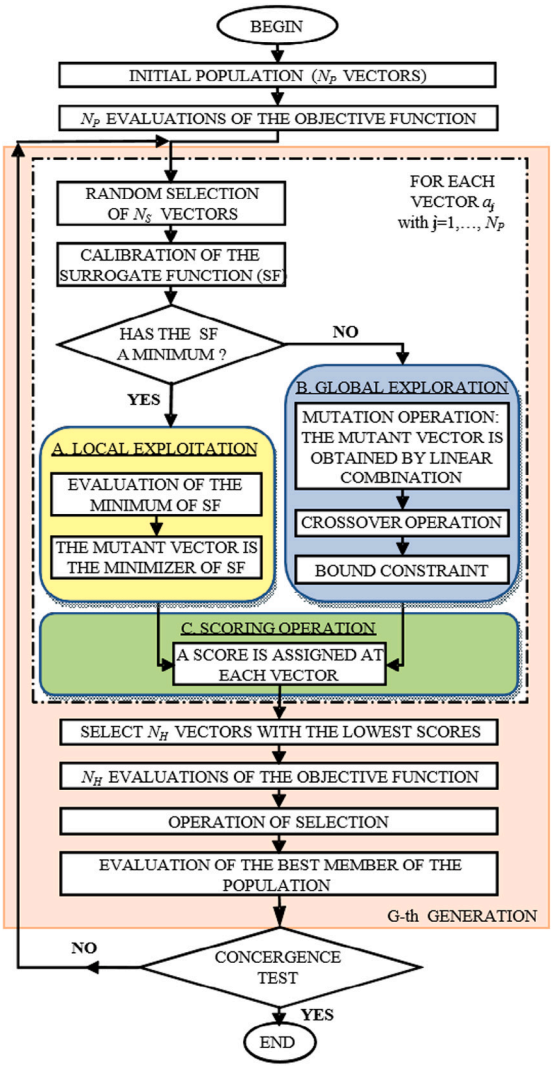

Fig. 4. Flowchart of the surrogate-assisted evolutionary algorithm.

where $\mathbf{Q}$ is a $D\times D$ matrix of quadratic coefficients and $\mathbf{l}$ is a $D\times 1$ vector of linear coefficients. The coefficients of the quadratic term matrix, of the linear term vector and of the constant c are estimated by applying the least square estimation method, i.e. by minimizing the squared sum of the differences between $\overline{H}(\mathbf{a}_{j,G})$ and $H(\mathbf{a}_{j,G})$ for the N_S selected points. If the surrogate function has a minimum, its minimizer $\bar{\mathbf{a}}$ is analytically obtained as:

$$\bar{\mathbf{a}} = -\mathbf{Q}^{-1}\mathbf{l} \tag{7}$$

and it is proposed as a candidate for the next generation.

To sum up, a candidate vector $\bar{\mathbf{a}}$ is obtained for each of the N_P groups. It is evaluated according to Eq. (7) or through the classic linear combination of vectors depending on whether the surrogate has a minimum or not. A score is then assigned to each candidate vector $\bar{\mathbf{a}}$ according to the criteria described in Section 3.1.2 and the objective function values are evaluated through Eq. (2) for the candidate vectors presenting the lower scores.

3.1.2. Scoring operation

The scoring operation is performed to assign a score to each candidate. The score S is defined as the weighted sum of two criteria. The first criterion depends on the objective function value predicted by the surrogate $\overline{H}(\mathbf{a}_{j,G})$ and the related score S_1 is computed as:

$$S_1 = 1 - \exp\left(-\frac{\overline{H}(\mathbf{a}_{j,G})^2}{H_{\text{best}}H_{\min,s}}\right) \tag{8}$$

where H_{best} is the minimum objective function value obtained until the current generation and $H_{\min,s}$ is the minimum among the objective function values evaluated for the N_S points selected to calibrate the surrogate. The lower the predicted value s_f is, the smaller the score S_1 of the candidate is.

According to the second criterion, the score S_2 depends on the distances of the candidate from the points for which the objective function has been already evaluated. For this purpose, the database created within the procedure is used. In this case, in order to ensure a global exploration of the research domain, the farther the parameter vector is from the already evaluated points, the lower is the score S_2. The score S_2 is defined as follow:

$$S_2 = 1 - \frac{\Delta_{min}}{\Delta_{max}} \tag{9}$$

where Δ_{min} and Δ_{max} are the minimum and the maximum distance between the candidate and all already evaluated points.

The two scores are combined with a weighted sum as $\alpha_1 S_1 + \alpha_2 S_2$, where α_1 and α_2 are weights. α_1 and α_2 are chosen in the range $0\leq\ \alpha_1, \alpha_2\ \leq 1$, with $\alpha_1 + \alpha_2 = 1$. If α_2 is close to one, the global exploration prevails on the local search and the candidate points are mainly placed in a rather unexplored region of the parameter domain. Otherwise, if the value of α_1 is high, local exploitation is emphasized and the candidate points with low predicted objective function values are preferred. According to [25], two different sets of weights are fixed depending on the convexity of the response surface. In the case the surrogate has a minimum and the minimizer is the candidate for the next generation, a higher weight must be assigned to the first criterion, i.e. $\alpha_1 = 2/3$ and $\alpha_2 = 1/3$. In the case the surrogate research fails, weight values are set as $\alpha_1 = 0$ and $\alpha_2 = 1$, favoring the second criterion.

Only the first N_H candidates (with $N_H < N_P$) with the lower scores are selected for new evaluations. In this way, a very reduced number of new FE model resolutions are performed at each generation. This allows to improve the speed performance of the optimization algorithm while keeping high the number of candidates at each iteration. Having a high number of candidates at each iteration is fundamental to preserve the ability of the algorithm to find the global minimum also in complex optimization problems.

3.2. The proposed calibration procedure for multiple specimens

The proposed procedure aims at reducing the computational effort for the calibration of multiple specimens. Obviously, the resolution of the FE model (needed to find the force–CMOD curve in the present paper) for a given set of constitutive law parameters and for a given geometry will produce results that are independent from the experimental data. On the contrary, the objective function value changes if the numerical outcomes are compared to the results of different experiments. Starting from this consideration, all the numerical results obtained from the calibration of a single specimen are stored in the database (see Section 3.1). This latter is then used to calculate the objective function values for other specimens and to map the parameter domain using the points (i.e. $\mathbf{a}$ vectors) already investigated, thus avoiding to repeat FE analyses. This allows to speed up the convergence of the optimization algorithm as the database grows.

The proposed procedure can be summarized as follows:

- Apply the surrogate-assisted evolutionary algorithm for the calibration of the first specimen as described in Section 3.1. Randomly choose the initial vector population within the parameter space.

- Throughout the calibration process, store in a database the value of each parameter vector $\mathbf{a}_j$ investigated, the corresponding objective function value $H(\mathbf{a}_{j,G})$ and the force–CMOD curve produced by the FE analysis. The value of $H(\mathbf{a}_{j,G})$ is used within the calibration of the first specimen to guide the choice of the best candidates while the force–CMOD curve is used for the calibration of subsequent specimens.
- When the algorithm reaches the solution for the first specimen, store results in the database and select a new specimen to calibrate.
- For each parameter vector $\mathbf{a}_j$ that has been used to perform a FE analysis, calculate the new value of the objective function H by comparing the numerical force–CMOD curve contained in the database with the experimental curve for the new specimen, by means of Eq. (2).
- Select the initial population of N_P vectors for the calibration of the selected specimen in the following way. Two-thirds of the N_P vectors are chosen as those which have the lowest values of the objective function H. For the remaining population, choose vectors that ensure a well distributed population in the research space. For this purpose, use the score S_2 of Eq. (9) to select the best candidates.
- With the selected initial population, apply the surrogate-assisted evolutionary algorithm described in Section 3.1 to calibrate the constitutive law parameters of the current specimen. During the calibration, update the database with data on the new evaluations of the FE model.
- Repeat the procedure for all the other specimens.

A flowchart of the procedure can be found in Fig. 5.

The proposed procedure has several advantages. First, the use of a surrogate function coupled with an evolutionary algorithm allows to reach the optimal solution with a limited number of evaluations also in the case of multiple local minima [25]. On the contrary, a local optimization algorithm, such as a gradient-based algorithm, does not guarantee the convergence to the global minimum but it could converge to a local minimum depending on the chosen starting point. Moreover, the efficiency of local optimization algorithms rapidly decreases when the number of calibration parameters is greater than 3 or 4.

The use of a database allows to map the research space of new specimens and, consequently, to identify the region where the global minimum is more likely to be, without performing the large number of objective function evaluations typical of the first iterations of the procedure. Moreover, the use of the database helps the algorithm to avoid the resolution of the numerical model in already mapped regions and where the objective function has high values. This is done not only with reference to the research points in the current generation or within the single optimization problem, but it is also done by exploiting all the results obtained for the previous specimens. The parameter space mapping coupled with the polynomial surrogate also allows a very fast convergence if the current specimen has a force–CMOD curve not very different from one of the previously calibrated specimens. In this case, the second order polynomial function is able to locally fit the objective function and find a good solution also at the first iterations.

The same combination between the surrogate-assisted evolutionary algorithm and the database of results would have not been so easy if dealing with classic evolutionary or gradient-based algorithms. The main disadvantage of using evolutionary and genetic algorithms is that a large number of objective function evaluations are required to reach the global minimum. This is because they are based on a probabilistic search without information on the shape of the objective function. Moreover, as the calibration results obtained in the previous iterations and/or in the calibration of other specimens are not taken into account, usually new candidate vectors fall in some already investigated regions of the parameter domain.

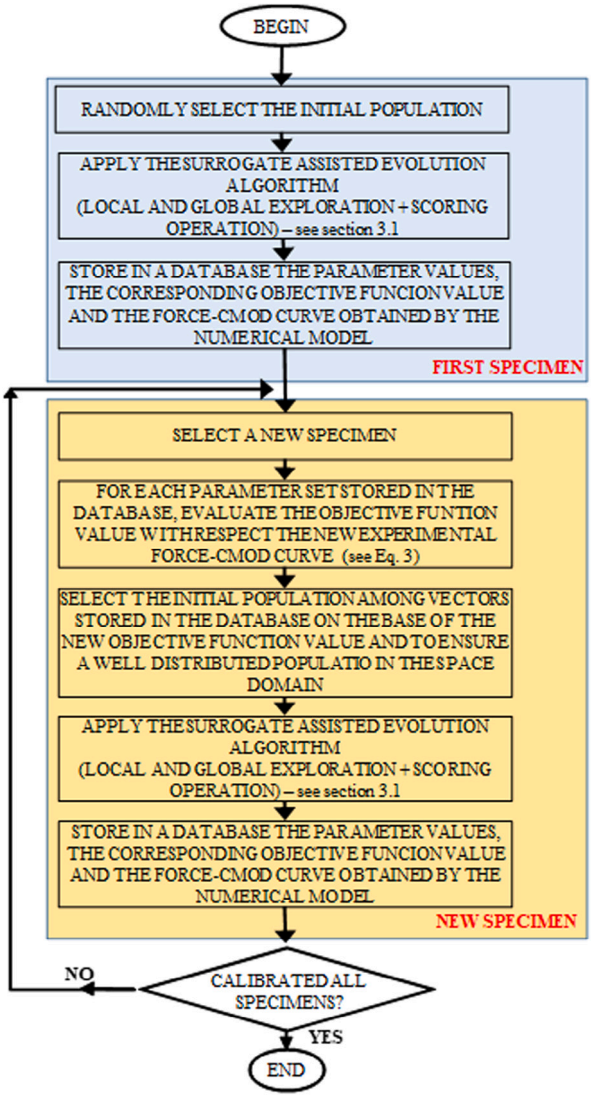

Fig. 5. Flowchart of the proposed procedure for the calibration of multiple specimens.

Gradient-based algorithms are guided from the gradient of the objective function and they account for the shape of the objective function only locally. No information about the objective function in regions that are far from the evaluated point is considered. A previous solution (i.e. the solution of a previously calibrated specimen) can be used as a starting point for the current calibration to have an advantage in terms of speed rate. However, the starting point could be inappropriate in the case of specimens with constitutive law not similar to the previous one and there is no guarantee to converge to the global minimum if the starting point is not close to it.

4. Results and discussion

The calibration procedure proposed in Section 3.2 is used to calibrate the parameters of the model in Eq. (1) for the 63 specimens described in Section 2.1. The 5 calibration parameters $a_1, \ldots, a_5$ are searched within the ranges reported in Table 1.

In order to obtain the coefficients of the second order polynomial function in a 5-dimensional space at least 21 points are needed. Consequently, a value of N_S greater than 21 is required. In this research, N_S is chosen equal to 26. The number of members of each population N_P and the number of new evaluations for each generation N_H are set

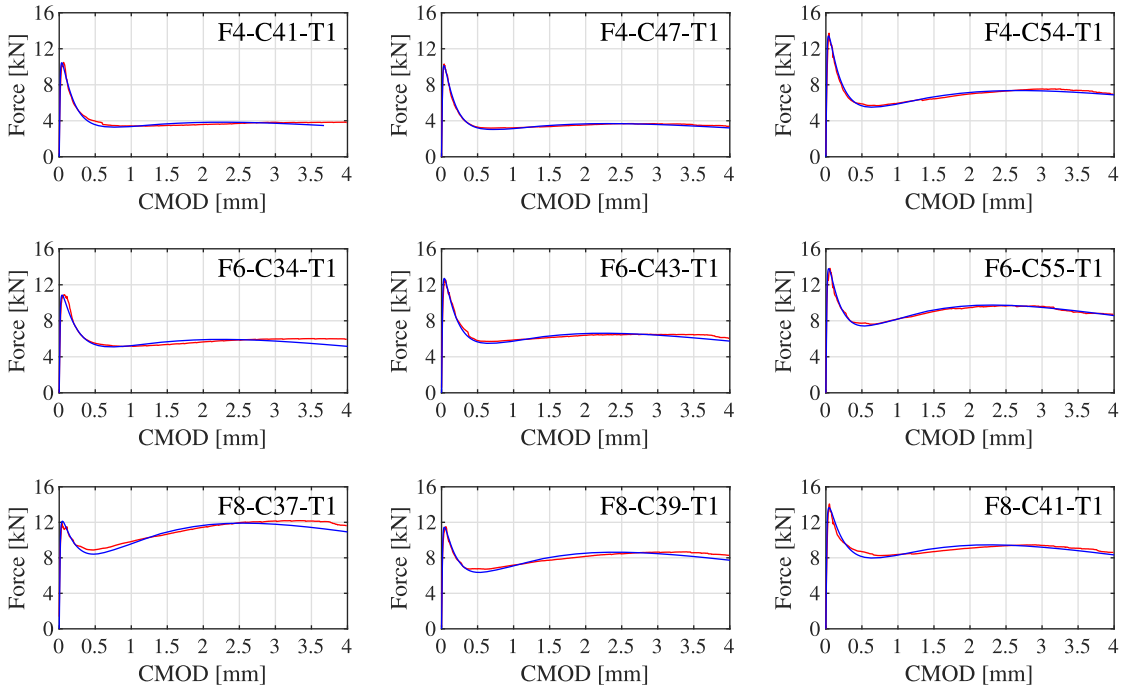

Fig. 6. Some examples of calibration results: experimental (red) vs numerical (blue) force–CMOD curves. (For interpretation of the references to color in this figure legend, the reader is referred to the web version of this article.)

Table 1
Search range for the constitutive law parameters.

	a_1 [MPa]	a_2 [1/mm]	a_3 [MPa]	a_4 [1/mm]	a_5 [1/mm]
Min value	+2.30	+6.50	+5.00	+0.39	+0.70
Max value	+4.50	+13.00	+7.80	+0.65	+3.00

equal to 38 and 4, respectively. The weights for the scoring operation are selected according to the strategy introduced in Section 3.1.2. The calibration process is stopped when at least two research points have the objective function value H less than 10^{-2} and their relative distance is less than 10^{-1}.

Fig. 6 shows examples of the obtained results in terms of force–CMOD curves. The numerical predictions (blue lines) almost perfectly match the experimental results (red lines). The number of objective function evaluations needed for the calibration of each specimen according to the proposed procedure is reported in Fig. 7(a). The specimen order of Fig. 7(a) corresponds to the order in which specimens have been calibrated. As far as the first specimen group (namely F4-C54) is concerned, we can note that the calibration of the first specimen is computationally demanding, while the calibrations of the other specimens of the same group are very fast. In particular, the number of required iterations goes from about 150 for the first specimen up to values lower than 10 (reaching even values of 1) for the other specimens of the same group. This is due to the fact that the target experimental curves are similar for specimens belonging to the same group. In this case, indeed, the data stored in the database (Section 3), populated during the calibration of the model for first specimens, allow to reduce the number of evaluations of the FE model. When the concrete strength and/or the fiber dosage change, the required number of evaluations slightly increases. In fact, the larger is the difference between the experimental curves of the current and previous specimen, the greater is the number of objective function evaluations required to reach the convergence since the distance between the minima of the objective function increases. In any case, the number of objective function evaluations required adopting the proposed procedure is significantly lower than that needed if the calibration procedure is separately applied for each specimen (Fig. 7(b)), namely without benefit from the result database. A total of 2285 objective function evaluations are required to calibrate all of the specimens with the proposed procedure while they become 9940 without exploiting the database, although the convergence criteria are the same.

The optimal values of the calibration parameters a_i are listed in Table 2. Results are averaged over the 7 specimens of each group. Parameter values for each specimen are graphically represented, together with their mean value, in Fig. 8. As expected, a global increase in the parameter a_1 (representative of the concrete tensile strength) with the concrete compressive strength can be observed. The peak of the second branch of the constitutive law depends on a combined effect of parameters a_3-a_5, which vary with the fiber dosage. The numerical stress–crack opening relationships obtained for each specimen group with the model parameters of Table 2 are presented in Fig. 9. As expected, greater concrete strengths lead to a higher curve peak, while the second stretch increases with the fiber dosage. Peak values of the first and second stretch of the mean curve for each specimen group are presented in Table 3.

The reduction in the computational effort does not compromise the calibration accuracy. This is demonstrated by the good correspondence between experimental and numerical results observed in Fig. 6 as well as in Table 4. In particular, Table 4 presents the absolute value of the errors e_F, e_A and $e_{\mathrm{CMOD}h}$ (see Section 2.3) averaged over the 7 specimens of each group. Besides the results presented in Fig. 6 and Table 4, the comparison between the experimental and numerical curves of each single specimen and the corresponding errors are presented in Table A.5 and Figs. A.10, A.11, A.12. This comparison confirms the good agreement between results.

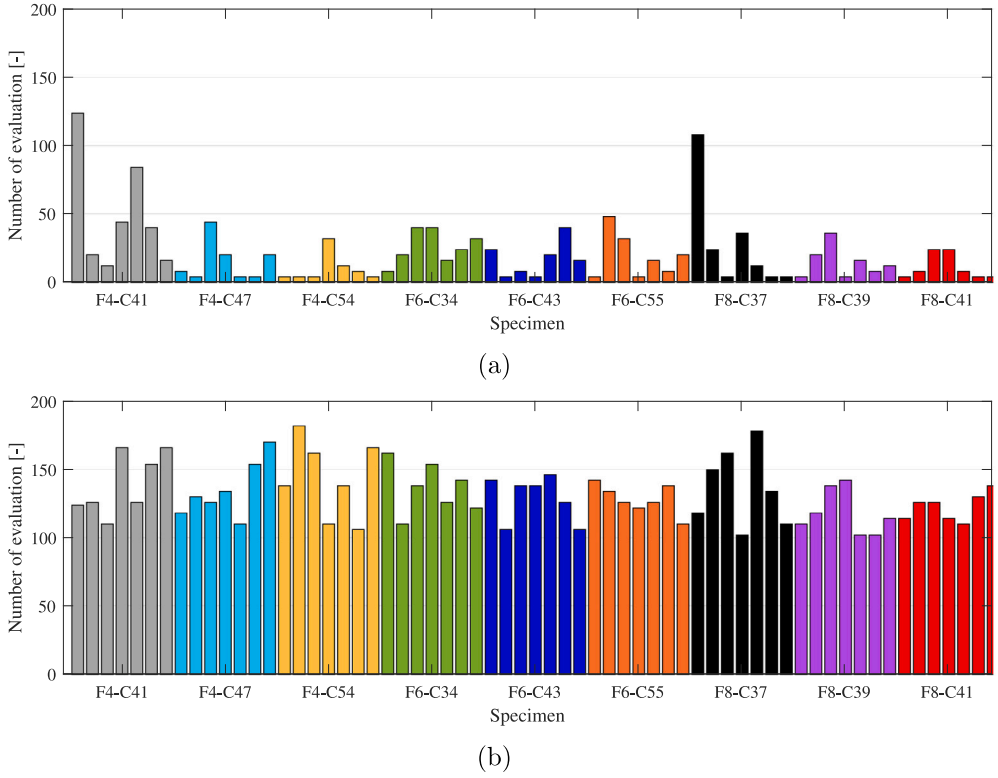

Fig. 7. Number of objective function evaluations: results obtained using (a) the proposed procedure for the calibration of multiple specimens and (b) the surrogate-assisted evolutionary algorithm applied separately for each specimen.

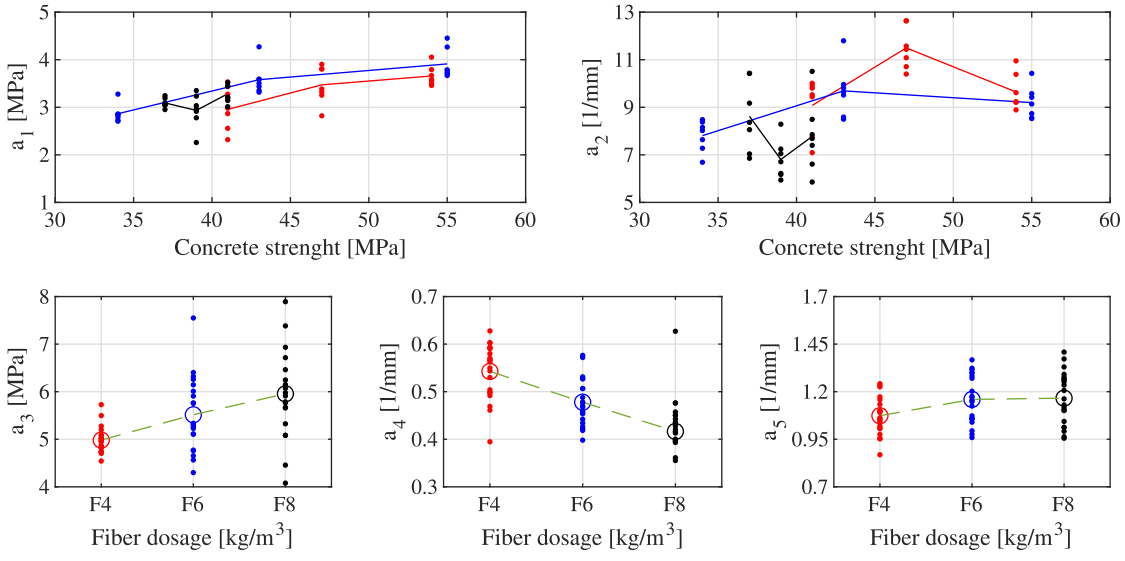

Fig. 8. Trend of the calibration parameters a_i: single values (markers) and mean trend (lines). Fiber dosages of 4 kg/m³ (red), 6 kg/m³ (blue) and 8 kg/m³ (black). (For interpretation of the references to color in this figure legend, the reader is referred to the web version of this article.)

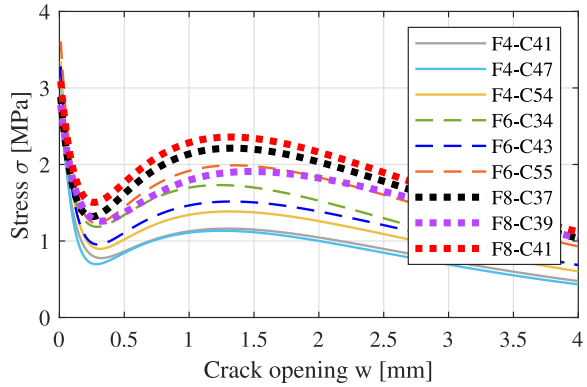

Fig. 9. Mean trend of the stress–CMOD curve for the different specimen groups. (For interpretation of the references to color in this figure legend, the reader is referred to the web version of this article.)

Table 2
Mean values of the calibration parameters a_i.

Specimen group	a_1 [MPa]	a_2 [1/mm]	a_3 [MPa]	a_4 [1/mm]	a_5 [1/mm]
F4-C41	+2.96	+9.08	+5.12	+0.55	+1.04
F4-C47	+3.47	+11.50	+4.94	+0.57	+1.08
F4-C54	+3.66	+9.64	+4.89	+0.50	+1.10
F6-C34	+2.86	+7.81	+5.70	+0.51	+1.20
F6-C43	+3.58	+9.69	+4.80	+0.47	+1.14
F6-C55	+3.91	+9.20	+6.04	+0.45	+1.14
F8-C37	+3.09	+8.62	+6.32	+0.44	+1.18
F8-C39	+2.93	+6.80	+5.43	+0.40	+1.07
F8-C41	+3.28	+7.77	+6.12	+0.42	+1.25

Table 3
Peak values of the stress–crack opening curves. σ_{peak1}: stress corresponding to the first peak; σ_{peak2} and w_{peak2}: stress and crack opening corresponding to the second peak, respectively.

Specimen group	σ_{peak1} [MPa]	σ_{peak2} [MPa]	w_{peak2} [mm]
F4-C41	+2.96	+1.16	+1.30
F4-C47	+3.47	+1.13	+1.25
F4-C54	+3.66	+1.39	+1.31
F6-C34	+2.86	+1.73	+1.24
F6-C43	+3.58	+1.52	+1.33
F6-C55	+3.91	+1.99	+1.34
F8-C37	+3.09	+2.21	+1.33
F8-C39	+2.93	+1.91	+1.48
F8-C41	+3.28	+2.36	+1.32

Table 4
Absolute values of the errors e_F, e_A and e_{CMOD_h} averaged over the 7 specimens of each group. e_{CMOD_h} is calculated for CMOD values of 0.5 and 2.5 mm.

Specimen group	e_F [%]	e_A [%]	$e_{CMOD0.5}$ [%]	$e_{CMOD2.5}$ [%]
F4-C41	+1.37	+0.25	+4.26	+1.11
F4-C47	+1.01	+0.48	+6.28	+0.76
F4-C54	+1.38	+0.19	+5.33	+1.07
F6-C34	+2.02	+0.59	+2.71	+1.71
F6-C43	+1.11	+0.46	+5.74	+2.01
F6-C55	+0.83	+0.41	+2.65	+1.23
F8-C37	+1.84	+0.54	+5.44	+0.87
F8-C39	+1.90	+0.41	+4.26	+2.11
F8-C41	+1.21	+0.32	+4.78	+1.51

5. Conclusions

This paper proposes a computationally efficient procedure to calibrate the model parameters of multiple specimens. The procedure combines the robustness in the global minimum search of a surrogate-assisted evolutionary algorithm with the exploitation of a database collecting the results of the previously calibrated specimens. In this way, the calibration of each new specimen can start from the database values rather than from randomly generated samples. This allows guiding the research of the optimal model parameters on the basis of the calibration results obtained for previous specimens, thus reducing the number of model evaluations required.

As an example, the procedure has been applied to the constitutive model calibration of multiple groups of fiber-reinforced concrete specimens. All the specimen groups are characterized by the same geometry but different concrete strength and/or fiber dosage. The constitutive model of each specimen is a cohesive crack model and its parameters are calibrated by minimizing the differences between the force–CMOD curve simulated by the model and the experimental counterpart obtained from a three-point bending test performed on the notched specimen.

The proposed procedure is compared with a classic calibration strategy that involves the separated calibration of each specimen without taking advantage of the result database. The proposed calibration procedure allows reducing the total number of model evaluations by about 4.5 times. Benefits are very remarkable for specimens of the same groups that have similar experimental curves, but also for specimens belonging to different groups. In this case, indeed, the mapping of the parameter space enables to have a more rich starting population and to significantly reduce the model evaluations also when the global minimum of the objective function for two subsequent calibrations moves in the parameter space.

This procedure is not limited to the experimental tests and the mechanical model presented in this work but it can be employed for the calibration of other mechanical models. It is particularly suited to the calibration of specimen groups characterized by nonlinear constitutive models due to the high computational effort needed to perform a large number of model simulations. The reduction in the computational burden does not compromise the calibration accuracy, as demonstrated by the good agreement between experimental and numerical results presented in the paper.

CRediT authorship contribution statement

Loris Vincenzi: Writing – review & editing, Writing – original draft, Validation, Software, Methodology, Data curation, Conceptualization. **Federico Ponsi:** Writing – review & editing, Writing – original draft, Validation, Methodology, Data curation, Conceptualization. **Elisa Bassoli:** Writing – review & editing, Writing – original draft, Validation, Methodology, Data curation, Conceptualization. **Nicola Buratti:** Writing – review & editing, Writing – original draft, Validation, Supervision, Project administration, Methodology, Data curation, Conceptualization.

Declaration of competing interest

The authors declare that they have no known competing financial interests or personal relationships that could have appeared to influence the work reported in this paper.

Data availability

Data will be made available on request.

Appendix

See Figs. A.10–A.12 and Table A.5

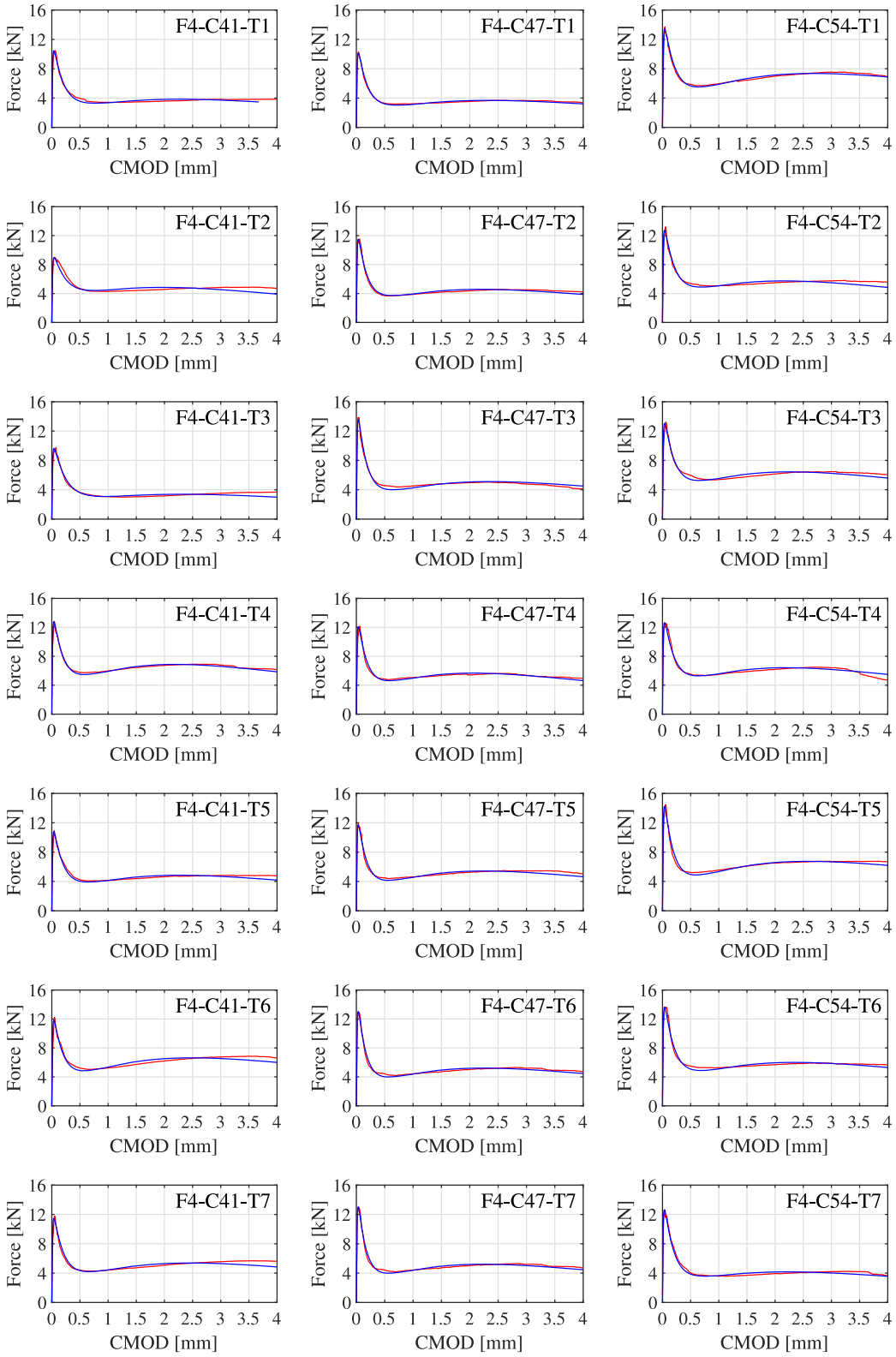

Fig. A.10. Results for specimens with fiber dosage of 4 kg/m^3. Red line: experimental curve; blue line: numerical curve. (For interpretation of the references to color in this figure legend, the reader is referred to the web version of this article.)

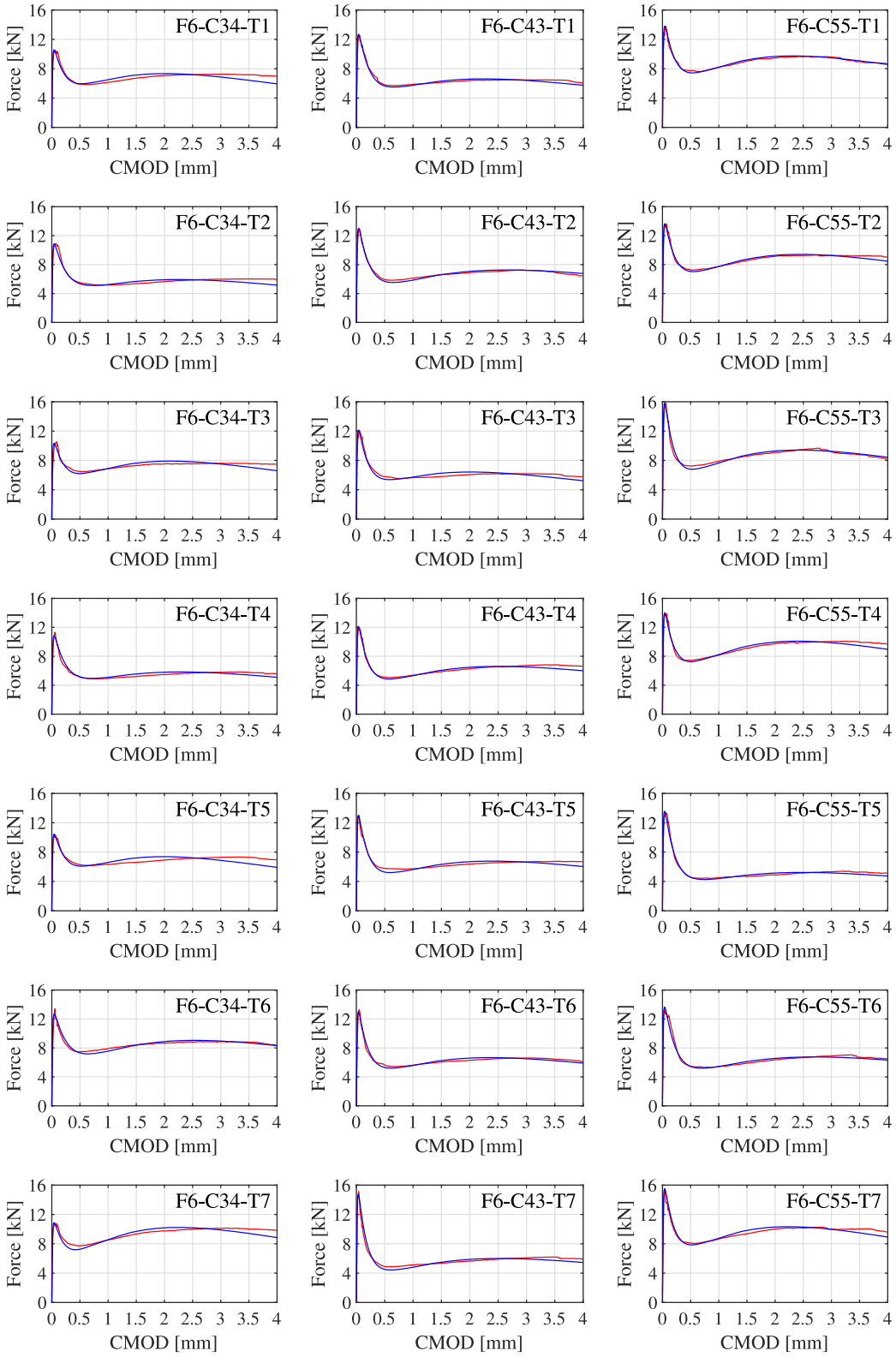

Fig. A.11. Results for specimens with fiber dosage of 6 kg/m^3. Red line: experimental curve; blue line: numerical curve. (For interpretation of the references to color in this figure legend, the reader is referred to the web version of this article.)

Table A.5
Errors e_F, e_A and e_{CMOD_h} for each single specimen. e_{CMOD_h} is calculated for CMOD values of 0.03, 0.05, 0.1, 0.2, 0.5, 1.5, 2.5, and 3.5 mm.

Specimen	e_F [%]	e_A [%]	$e_{CMOD0.03}$ [%]	$e_{CMOD0.05}$ [%]	$e_{CMOD0.1}$ [%]	$e_{CMOD0.2}$ [%]	$e_{CMOD0.5}$ [%]	$e_{CMOD1.5}$ [%]	$e_{CMOD2.5}$ [%]	$e_{CMOD3.5}$ [%]
F4-C41-T1	+0.33	+0.10	−6.83	+0.08	−0.82	−4.31	+10.13	−5.15	−2.91	+7.18
F4-C41-T2	+0.30	+0.42	−6.46	+0.94	+3.56	+11.28	+1.23	−7.67	−0.15	+12.78
F4-C41-T3	+1.32	−0.03	−9.58	−1.13	+1.56	−2.26	+1.06	−6.50	−0.49	+13.08
F4-C41-T4	+0.32	+0.62	−8.61	−2.96	−1.33	−1.92	+4.22	−1.82	+1.12	+0.91
F4-C41-T5	+1.32	+0.38	−7.94	−1.12	−3.14	+4.42	+4.92	−4.60	−1.82	+7.30
F4-C41-T6	+3.29	−0.03	−15.73	+4.60	−4.39	+4.19	+6.52	−6.54	−1.12	+8.02
F4-C41-T7	+2.68	−0.20	−13.68	+4.70	−4.02	−8.27	+1.73	−5.31	−0.19	+10.07
F4-C47-T1	+1.85	+0.38	−0.18	+0.14	−2.10	−3.99	+2.78	−3.41	+0.13	+3.28
F4-C47-T2	+0.24	−0.90	−4.30	+1.10	+0.39	−4.86	−2.43	−4.53	−0.32	+4.83
F4-C47-T3	+2.30	+0.16	+2.30	+2.73	−8.53	−3.06	+9.77	+0.27	−2.80	−5.96
F4-C47-T4	+0.83	−0.18	−9.80	+2.02	+1.50	−8.85	+3.62	−2.81	+0.31	+2.49
F4-C47-T5	+1.55	+0.98	+0.28	+0.12	−1.21	−8.26	+7.34	−3.77	+1.01	+8.35
F4-C47-T6	−0.14	+0.37	−1.89	+2.90	−2.50	−10.58	+9.02	−4.79	+0.39	+3.17
F4-C47-T7	−0.14	+0.37	−1.89	+2.90	−2.50	−10.58	+9.02	−4.79	+0.39	+3.17
F4-C54-T1	+2.15	+0.00	−7.09	−1.97	−4.50	−3.82	+3.61	−3.28	−0.47	+3.06
F4-C54-T2	+3.42	+0.34	−9.27	+4.66	−6.34	−4.35	+5.53	−4.69	−0.56	+8.51
F4-C54-T3	+1.42	+0.07	−14.70	−1.05	+1.14	−2.22	+9.27	−5.97	+0.13	+5.61
F4-C54-T4	−0.88	+0.02	−5.12	+0.26	+6.59	−0.94	+2.12	−4.30	+0.74	−1.99
F4-C54-T5	+1.51	+0.45	−8.98	+3.57	−0.44	−10.58	+5.06	−0.81	−1.01	+3.83
F4-C54-T6	−0.18	+0.09	−5.77	+1.55	+6.69	−6.72	+7.47	−3.09	−2.49	+3.04
F4-C54-T7	+0.08	+0.38	−0.57	−5.78	+1.62	+6.10	+4.28	−7.81	−2.12	+9.32
F6-C34-T1	−0.68	−0.28	−5.67	−2.12	+6.99	+4.27	−0.72	−6.31	−0.23	+10.56
F6-C34-T2	+0.31	+0.39	−7.22	−0.84	+7.53	+0.25	+2.88	−5.57	−0.48	+8.93
F6-C34-T3	+1.98	−0.52	−17.27	+0.65	+6.59	−0.81	+4.30	−4.46	−3.47	+5.96
F6-C34-T4	+4.28	−1.99	−4.99	+4.54	−1.41	−9.68	+0.04	−6.53	−2.26	+6.59
F6-C34-T5	+0.64	−0.52	−3.02	−3.45	+3.52	+1.25	+3.19	−9.18	−1.01	+11.85
F6-C34-T6	+5.45	−0.14	−12.61	+3.55	−5.58	−5.68	+1.87	+0.64	−2.44	+0.78
F6-C34-T7	−0.78	+0.29	−4.29	−0.98	+4.65	+5.64	+5.95	−3.73	−2.05	+5.62
F6-C43-T1	−0.95	+0.44	−7.35	−1.86	−1.10	+0.55	+2.50	−2.69	−2.15	+5.10
F6-C43-T2	+0.70	+0.42	−7.26	+0.99	−3.29	−1.88	+4.25	+0.56	−2.60	−1.49
F6-C43-T3	−0.11	−0.31	−8.26	+1.38	+6.11	+2.03	+6.54	−7.77	−1.89	+7.90
F6-C43-T4	+0.13	+0.61	−6.36	−0.69	+2.19	−2.59	+4.19	−3.22	−0.62	+7.65
F6-C43-T5	+0.62	−0.14	−1.26	+1.64	−7.25	−0.75	+8.64	−4.05	−3.38	+5.39
F6-C43-T6	+2.49	−0.58	−6.47	+3.77	−4.00	−7.65	+6.23	−3.23	−1.98	+3.21
F6-C43-T7	+2.73	+0.74	−0.28	+1.21	−12.14	−9.79	+7.82	−2.89	−1.45	+7.41
F6-C55-T1	+0.24	−0.45	−4.41	−0.57	−4.75	−1.32	+3.73	−1.72	−0.81	−1.13
F6-C55-T2	+0.23	−0.12	−4.18	−1.24	+2.32	−2.63	+2.83	−2.14	−1.60	+3.16
F6-C55-T3	+0.63	+0.18	−8.63	+0.60	+0.69	−8.70	+6.04	−1.63	+0.74	−1.44
F6-C55-T4	+0.69	−0.31	−0.94	−0.41	+4.38	−3.49	+2.40	−2.96	−1.51	+4.86
F6-C55-T5	−1.61	+0.44	−7.25	−1.34	+5.65	−2.08	+0.05	−4.54	−1.82	+5.73
F6-C55-T6	−1.88	+0.34	−2.50	−4.07	+4.38	+7.05	+0.48	−3.75	−0.90	+2.43
F6-C55-T7	−0.56	−1.00	−3.44	−4.35	−6.67	−4.02	+3.04	−4.81	−1.25	+5.45
F8-C37-T1	+0.60	+1.38	−4.46	−5.07	−0.87	+0.64	+5.50	−2.25	+0.53	+5.90
F8-C37-T2	+1.12	+0.12	−0.43	+0.69	−3.03	−4.87	+6.88	−3.94	−1.38	+4.83
F8-C37-T3	+3.59	−0.50	−6.75	−7.47	−4.70	−0.60	+6.20	−5.97	−0.56	+3.54
F8-C37-T4	+2.03	−0.53	−7.05	−3.48	−8.53	+1.56	+3.71	−3.49	−1.53	+4.18
F8-C37-T5	+2.67	−0.28	−17.45	−6.01	−5.99	−8.33	+5.84	−3.94	−0.63	+5.21
F8-C37-T6	+1.12	+0.12	−0.43	+0.69	−3.03	−4.87	+6.88	−3.94	−1.38	+4.83
F8-C37-T7	−1.79	+0.83	−9.94	−6.98	+1.72	+7.00	+3.07	−1.94	+0.09	+4.20
F8-C39-T1	+0.60	−0.13	−7.03	−0.64	−3.88	−1.92	+6.16	−3.81	−1.99	+5.02
F8-C39-T2	+3.85	+0.30	−14.69	+3.39	−2.68	−6.57	+7.37	−0.24	−2.28	+1.78
F8-C39-T3	−1.95	−1.67	−11.62	−3.05	−3.19	−6.40	+1.92	−0.64	−3.93	−1.36
F8-C39-T4	+1.95	−0.37	−14.99	+0.18	+7.63	+4.06	+0.23	−7.19	+0.02	+8.04
F8-C39-T5	+0.35	+0.12	−2.37	+0.22	−0.68	−6.25	+6.64	−1.75	−1.99	+2.50
F8-C39-T6	+2.69	−0.13	−14.63	−0.21	+4.94	−4.36	−0.47	−0.60	−0.96	+1.75
F8-C39-T7	+1.89	+0.18	−9.53	−6.66	+1.46	+1.99	+7.07	−1.09	−3.60	+1.08
F8-C41-T1	+2.97	−0.16	−6.45	+3.13	−6.96	−4.56	+6.33	−3.94	−0.67	+3.04
F8-C41-T2	+1.36	+0.01	−8.93	+1.23	+0.14	−3.51	+3.92	−1.45	−1.10	+2.42
F8-C41-T3	+1.14	+0.45	−4.60	+1.57	−3.52	−4.11	+5.37	−2.59	−0.51	+2.15
F8-C41-T4	+0.80	+0.06	−12.20	−0.60	+2.77	+4.55	+2.63	−3.50	−0.91	+2.99
F8-C41-T5	−0.29	−0.55	−0.79	+0.19	−7.18	+0.52	+7.60	−5.08	−2.64	+6.53
F8-C41-T6	+1.29	+0.55	−9.67	−0.37	−5.86	−0.50	+3.44	−1.46	+3.00	−0.51
F8-C41-T7	−0.64	−0.50	−4.34	−1.64	−2.01	−1.55	+4.14	−2.88	−1.72	+0.65

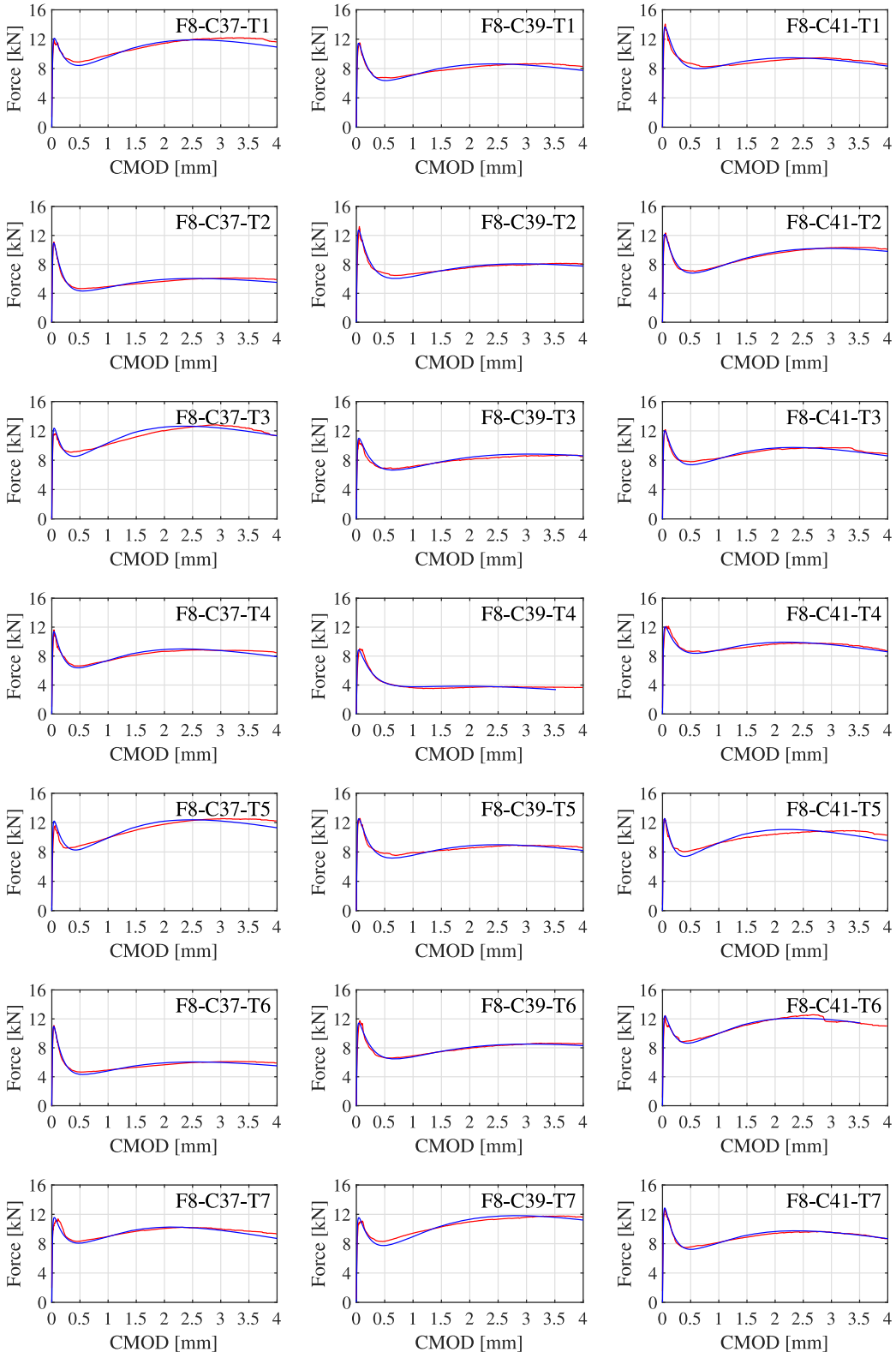

Fig. A.12. Results for specimens with fiber dosage of 8 kg/m^3. Red line: experimental curve; blue line: numerical curve. (For interpretation of the references to color in this figure legend, the reader is referred to the web version of this article.)

References

[1] M. Tanaka, G.S. Dulikravich, Inverse Problems in Engineering Mechanics, Elsevier, 1998.

[2] A. Nour, B. Massicotte, R. de Montaignac, J.-P. Charron, Development of an inverse analysis procedure for the characterisation of softening diagrams for FRC beams and panels, Constr. Build. Mater. 94 (2015) 35–44, http://dx.doi.org/10.1016/j.conbuildmat.2015.06.049, URL https://www.sciencedirect.com/science/article/pii/S0950061815300064.

[3] S.J. Stephen, B. Raphael, R. Gettu, S. Jose, Determination of the tensile constitutive relations of fiber reinforced concrete using inverse analysis, Constr. Build. Mater. 195 (2019) 405–414, http://dx.doi.org/10.1016/j.

conbuildmat.2018.11.014, URL https://www.sciencedirect.com/science/article/pii/S0950061818326795.
[4] V.S. Gopalaratnam, S.P. Shah, Tensile failure of steel fiber-reinforced mortar, J. Eng. Mech. 113 (5) (1987) 635–652, http://dx.doi.org/10.1061/(ASCE)0733-9399(1987)113:5(635).
[5] S.P. Shah, A. Carpinteri, Fracture mechanics test methods for concrete: report of Technical Committee 89-FMT Fracture Mechanics of Concrete, Test Methods, RILEM (the International Union of Testing and Research Laboratories for Materials and Structures), 1991.
[6] G. Bolzon, R. Fedele, G. Maier, Parameter identification by Kalman filter of a cohesive crack model, Comput. Methods Appl. Mech. Engrg. 191 (2002) 2847–2871.
[7] J.-K. Kim, Y. Lee, S.-T. Yi, Fracture characteristics of concrete at early ages, Cem. Concr. Res. 34 (3) (2004) 507–519, http://dx.doi.org/10.1016/j.cemconres.2003.09.011.
[8] S.H. Kwon, Z. Zhao, S.P. Shah, Effect of specimen size on fracture energy and softening curve of concrete: Part II. Inverse analysis and softening curve, Cem. Concr. Res. 38 (8) (2008) 1061–1069, http://dx.doi.org/10.1016/j.cemconres.2008.03.014.
[9] J. Olesen, Fictitious crack propagation in fiber-reinforced concrete beams, J. Eng. Mech. 127 (3) (2001) 272–280.
[10] L. Ostergaard, J. Olesen, Comparative study of fracture mechanical test methods for concrete, Fract. Mech. Concrete Struct. 1 (2004) 455–462.
[11] J. Barros, V. Cunha, A. Ribeiro, J. Antunes, Post-cracking behaviour of steel fibre reinforced concrete, Mater. Struct./Materiaux et Constructions 38 (275) (2005) 47–56, http://dx.doi.org/10.1617/14058.
[12] J.L.A. de Oliveira e Sousa, R. Gettu, Determining the tensile stress-crack opening curve of concrete by inverse analysis, J. Eng. Mech. 132 (2) (2006) 141–148, http://dx.doi.org/10.1061/(ASCE)0733-9399(2006)132:2(141).
[13] K. Chiranjeevi Reddy, K.V. Subramaniam, Analysis for multi-linear stress-crack opening cohesive relationship: Application to macro-synthetic fiber reinforced concrete, Eng. Fract. Mech. 169 (2017) 128–145, http://dx.doi.org/10.1016/j.engfracmech.2016.11.015.
[14] M. Alberti, A. Enfedaque, J. Gálvez, E. Reyes, Numerical modelling of the fracture of polyolefin fibre reinforced concrete by using a cohesive fracture approach, Composites B 111 (2017) 200–210, http://dx.doi.org/10.1016/j.compositesb.2016.11.052.
[15] A. Hillerborg, Analysis of fracture by means of the fictious crack model, particularly for fiber-reinforced concrete, In. J. Cement Compos. Lightweight Concrete 2 (4) (1980) 177–184.
[16] Z. Bazant, B. Oh, Crack band theory for fracture of concrete, Matériaux et Constructions 16 (1983) 155–177, http://dx.doi.org/10.1007/BF02486267.
[17] I. Löfgren, H. Stang, J. Olesen, Fracture properties of FRC determined through inverse analysis of wedge splitting and three-point bending tests, J. Adv. Concrete Technol. 3 (2005) 423–434, http://dx.doi.org/10.3151/jact.3.423.
[18] A.B. Bhosale, C. Lakavath, S. Suriya Prakash, Multi-linear tensile stress-crack width relationships for hybrid fibre reinforced concrete using inverse analysis and digital image correlation, Eng. Struct. 225 (2020) 111275, http://dx.doi.org/10.1016/j.engstruct.2020.111275.
[19] W. Nana, H. Tran, T. Goubin, G. Kubisztal, A. Bennani, T. Bui, G. Cardia, A. Limam, Behaviour of macro-synthetic fibers reinforced concrete: Experimental, numerical and design code investigations, Structures 32 (2021) 1271–1286, http://dx.doi.org/10.1016/j.istruc.2021.03.080.
[20] F. Tin-Loi, N. Que, Identification of cohesive crack fracture parameters by evolutionary search, Comput. Methods Appl. Mech. Engrg. 191 (49) (2002) 5741–5760, http://dx.doi.org/10.1016/S0045-7825(02)00483-8.
[21] N. Buratti, C. Mazzotti, M. Savoia, Post-cracking behaviour of steel and macro-synthetic fibre-reinforced concretes, Constr. Build. Mater. 25 (5) (2011) 2713–2722.
[22] M.S. Jepsen, L. Damkilde, I. Lövgren, A fully general and adaptive inverse analysis method for cementitious materials, Mater. Struct. 49 (10) (2016) 4335–4348, http://dx.doi.org/10.1617/s11527-015-0791-3.
[23] Y.T. Trindade, L.A. Bitencourt Jr., O.L. Manzoli, Design of SFRC members aided by a multiscale model: Part II – predicting the behavior of RC-SFRC beams, Compos. Struct. 241 (2020) 112079, http://dx.doi.org/10.1016/j.compstruct.2020.112079, URL https://www.sciencedirect.com/science/article/pii/S0263822319325474.
[24] C. Del Prete, I. Boumakis, R. Wan-Wendner, J. Vorel, N. Buratti, C. Mazzotti, A lattice discrete particle model to simulate the viscoelastic behaviour of macro – synthetic fibre reinforced concrete, Constr. Build. Mater. 295 (2021) 123630, http://dx.doi.org/10.1016/j.conbuildmat.2021.123630, URL https://www.sciencedirect.com/science/article/pii/S0950061821013908.
[25] L. Vincenzi, P. Gambarelli, A proper infill sampling strategy for improving the speed performance of a surrogate-assisted evolutionary algorithm, Comput. Struct. 178 (2017) 58–70, http://dx.doi.org/10.1016/j.compstruc.2016.10.004.
[26] B. Titurus, M.I. Friswell, Regularization in model updating, Internat. J. Numer. Methods Engrg. 75 (4) (2008) 440–478.
[27] M. Lee, B. Barr, A four-exponential model to describe the behaviour of fibre reinforced concrete, Mater. Struct. 37 (7) (2004) 464–471, http://dx.doi.org/10.1007/BF02481583.
[28] A. Blanco, P. Pujadas, A. de la Fuente, S. Cavalaro, A. Aguado, Application of constitutive models in European codes to RC–FRC, Constr. Build. Mater. 40 (2013) 246–259, http://dx.doi.org/10.1016/j.conbuildmat.2012.09.096, URL http://www.sciencedirect.com/science/article/pii/S095006181200774X.
[29] C. Jin, N. Buratti, M. Stacchini, M. Savoia, G. Cusatis, Lattice discrete particle modeling of fiber reinforced concrete: Experiments and simulations, Eur. J. Mech. A Solids 57 (2016) 85–107, http://dx.doi.org/10.1016/j.euromechsol.2015.12.002.
[30] M.L. Mineiro, R. Monte, O.L. Manzoli, L.A. Bitencourt, An integrated experimental and multiscale numerical methodology for modeling pullout of hooked-end steel fiber from cementitious matrix, Constr. Build. Mater. 344 (2022) 128215, http://dx.doi.org/10.1016/j.conbuildmat.2022.128215, URL https://www.sciencedirect.com/science/article/pii/S0950061822018785.
[31] M. Savoia, L. Vincenzi, Differential evolution algorithm for dynamic structural identification, J. Earthq. Eng. 12 (5) (2008) 800–821.
[32] M. Savoia, B. Ferracuti, L. Vincenzi, Inverse analysis for the calibration of FRP - Concrete interface law, Adv. Struct. Eng. 12 (5) (2009) 613–625.
[33] L. Vincenzi, M. Savoia, Coupling response surface and differential evolution for parameter identification problems, Comput.-Aided Civ. Infrastruct. Eng. 30 (5) (2015) 376–393, http://dx.doi.org/10.1111/mice.12124.
[34] R. Storn, K. Price, Differential evolution - a simple and efficient heuristic for global optimization over continuous spaces, J. Global Optim. 11 (1997) 341–359.